

Observations and interpretations of high-frequency volcanic tremor produced under varying seismic-acoustic amplitude ratios on Mt. Etna

Maurice Weber *1, Christopher J. Bean 1, Ivan Lokmer 2, Silvio De Angelis 3,4, Luciano Zuccarello 4,3 *Corresponding author

- 1 Dublin Institute for Advanced Studies, Dublin, Ireland
- 2 University College Dublin, Dublin, Ireland
- 3 University of Liverpool, Liverpool, UK
- 4 Istituto Nazionale di Geofisica e Vulcanologia, Sezione di Pisa, Pisa, Italy

Email addresses:

mweber@cp.dias.ie (Maurice Weber) chris.bean@dias.ie (Christopher J. Bean) ivan.lokmer@ucd.ie (Ivan Lokmer) silvioda@liverpool.ac.uk (Silvio De Angelis) luciano.zuccarello@ingv.it (Luciano Zuccarello) Highlights

- Unprecedented high-resolution seismic dataset from summit of Mount Etna
- Revealing rare high-frequency seismic tremor in short-duration episodes
- Seismic tremor produced under varying acoustic conditions

Observations and interpretations of high-frequency volcanic tremor produced under varying seismic-acoustic amplitude ratios on Mt. Etna

Maurice Weber^{a,*}, Christopher J. Bean^a, Ivan Lokmer^b, Silvio De Angelis^{c,d}, Luciano Zuccarello^{d,c}

^aDublin Institute for Advanced Studies, Dublin, Ireland
^bUniversity College Dublin, Dublin, Ireland
^cUniversity of Liverpool, Liverpool, UK
^dInstituto Nazionale di Geofisica e Vulcanologia, Sezione di Pisa, Pisa, Italy

Abstract

We present a comprehensive, high-resolution seismic-acoustic dataset from Mt. Etna acquired through a large, unprecedented deployment of seismometers and microphones in the summit region, highlighting rarely reported high-frequency (12-15Hz), short-duration volcanic tremor episodes. These events exhibit variable seismic-acoustic amplitude ratios, implying multiple triggering mechanisms. Our analysis suggests that while some tremor occurrences are indirectly associated with degassing processes — evidenced by coincident acoustic signals at different distinct frequencies — others lack any acoustic counterpart, indicating that degassing and thus fluid migration are not a necessary condition for tremor generation. We propose that in addition to traditional models requiring fluid movement for tremor generation, quasi-brittle, mesoscale failure within weak edifice material may act as a direct source mechanism radiating high-frequency tremor. This interpretation aligns with prior studies and helps explain shallow seismic tremor episodes in the absence of acoustic signals.

Keywords: volcanoes, seismic tremor, high spectral frequencies, driving processes, seismic-acoustic correlations

1. Introduction

- Seismic tremor is considered a critical parameter for volcano monitoring, able to provide valuable insights into the state of activity at volcanoes (e.g. [1] or more recently [2]) and
- considered an important tool to support eruption forecasting ([3]). Understanding the processes
- 5 that generate the broad range of tremor signals recorded at volcanoes ([1]) is essential; yet, a
- 6 comprehensive understanding of their source mechanisms remains elusive (e.g. [2]).
- In this study we examine high-frequency volcanic tremor (i.e., at frequencies > 10Hz) with
- 8 the aim to shed light on rarely investigated frequency ranges. Volcanic tremor is typically
- found at frequencies between 0.1 and 10Hz ([4]). Due to the close proximity (< 1km) to
- the source required to record tremor above 10Hz, these higher frequency signals > 10Hz are
- typically overlooked [5]. Analysis and location of high-frequency tremor is further complicated
- by highly complex waveforms lacking phase arrivals [6] as well as significant scattering at higher
- is a significant waveforms facilities and the significant sections as in significant

frequencies from the heterogeneous volcanic edifice [7]. Here, we focus on high-frequency tremor

^{*}Corresponding author

signals recorded at Mt. Etna. Dominant tremor frequencies at Etna are typically reported at $\sim 3Hz$ with energy generally concentrated between 0.5 and 5Hz ([8]). Except for a few notable studies (e.g., [9]) little investigation has been carried out on tremor at frequencies >10Hz at Mt. Etna.

This lack of coverage motivates this study where we focus on rarely investigated high frequency ranges attempting to shed further light on the complex processes triggering volcanic tremor.

2. Data

Two campaigns were conducted within the summit region of Mt. Etna during the summer 21 of 2022. These campaigns involved the deployment of six arrays of short-period seismometers 22 (SMARTSOLO nodes, 5Hz) with approximately circular geometry, each comprising between 9 23 and 25 instruments. In addition, a linear array including 4 broadband seismometers (Guralp, 24 60s-50Hz) and 7 infrasound sensors (Nanometrics, Trillium Compact 120s) was installed. During the first campaign, in July 2022, the linear array was installed, which remained operational 26 for 50 days. Later, during the second campaign, between 25th August and 1st September, 27 the circular arrays (SMARTSOLO nodes, 5Hz) were deployed and extended the linear array 28 towards the Bocca Nuova Crater (BNC) with the addition of 4 short-period stations (SMART-29 SOLO nodes, 5Hz). 30 This deployment was unprecedented at Etna for its size, station density and coverage of the 31 summit area, and particularly well-suited for the investigation of high-frequency tremor above 10 Hz. A map showing the distribution of stations is found in figures 2.1.

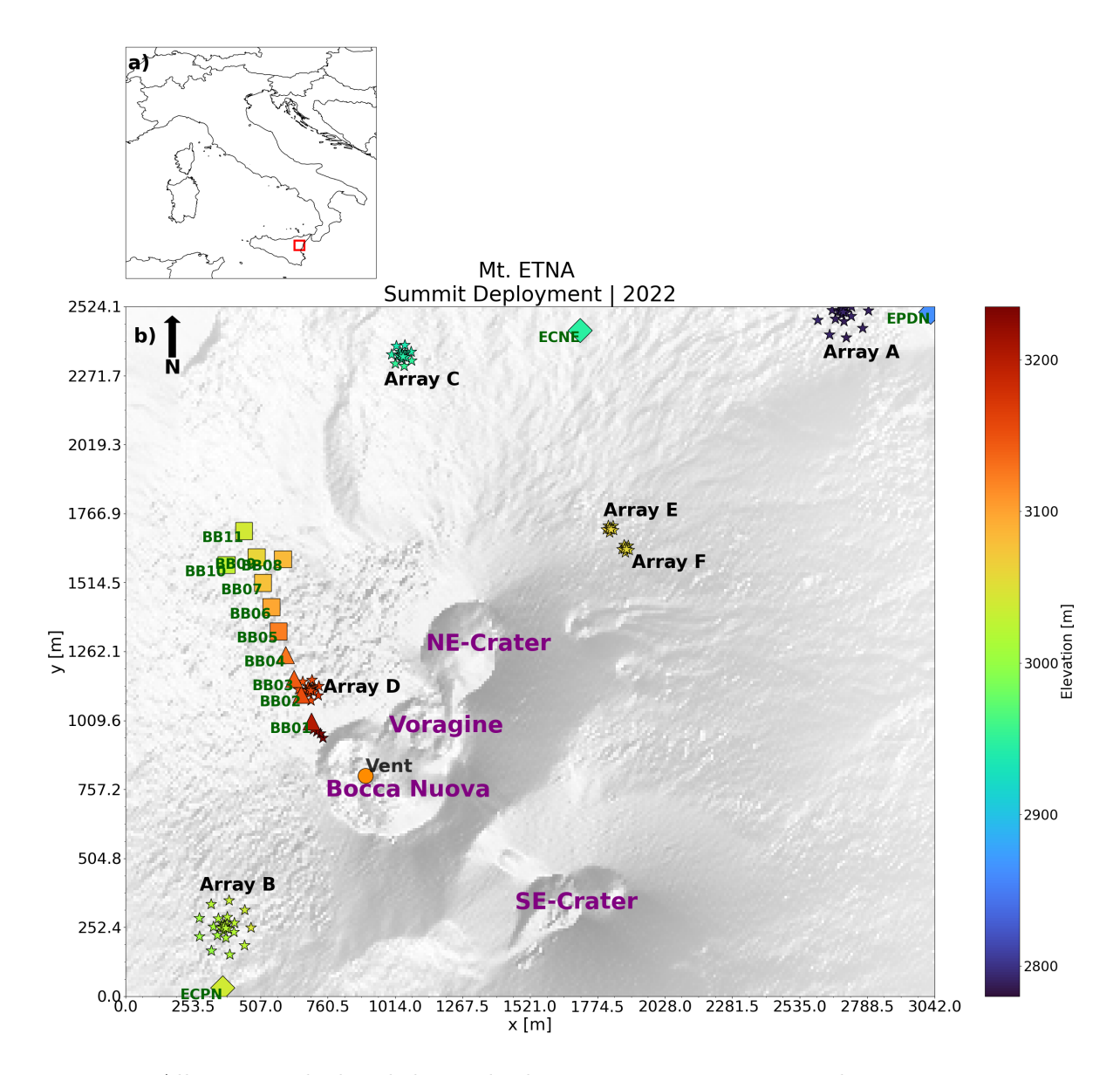
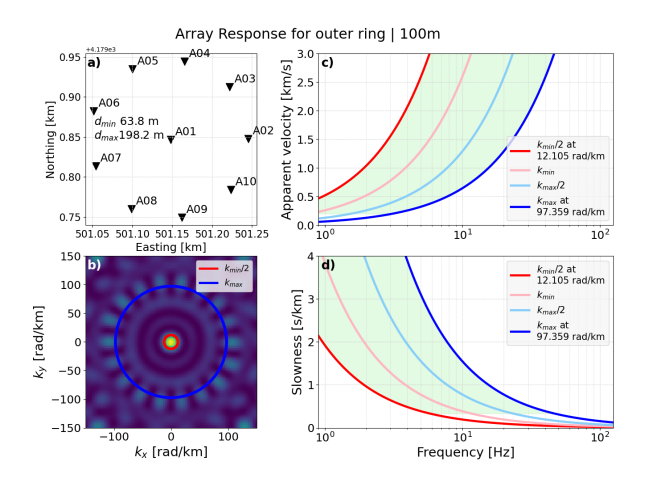


Figure 2.1: All stations deployed during both campaigns to Mt. Etna during summer 2022 seen in Panel (b) with an indication of the location of Mt. Etna in panel (a). All short-period stations are represented by stars, installed in six circular Arrays (A-F) as well as near the BNC. In addition, a linear array of broadband stations (BB01-BB04) and 7 infrasound stations (BB05-BB11) were deployed in an north-north-western direction leading away from BNC. Three stations (ECPN, ECNE, EPDN) of the permanent network operated by Instituto Nazionale di Geofisica e Vulcanologia (INGV) are also indicated.

The circular arrays were designed to capture a broad range of frequencies. This was achieved by constructing up to four concentric rings of instruments around a central element with the radius of these rings increasing from only 5 m for the innermost ring to 100 m for the outermost ring, resulting in a maximum aperture of 200 m. While the inner ring only consisted of 3 stations the outer one was made up of 9 stations amounting to 25 stations in total. The varying radius of the rings and range of inter-station distances allowed an array response 1-5Hz and up to $\sim 100Hz$ (see figures 2.2 and 2.3). Even though the SMARTSOLO nodes' response begins to fall off at 5 Hz the instrument's sensitivity is still sufficient down to < 1Hz which is still covered by the array's response. Similarly, the upper end of the response matches the Nyquist-frequency

at $125\ Hz$. Our main frequency band of interest is $10\text{-}20\ Hz$ and therefore well covered by the array configuration. With 104 short-period stations available in total, two arrays were constructed with the full 25-station configuration as described while the remaining arrays were scaled down. Two arrays were missing the outer ring of 9 stations, which reduced the number of stations in those arrays to 16 with a maximum aperture of $80\ m$, while for the remaining two arrays the third ring consisting of 7 stations was also removed leaving just 9 stations and a maximum aperture of only $30\ m$.



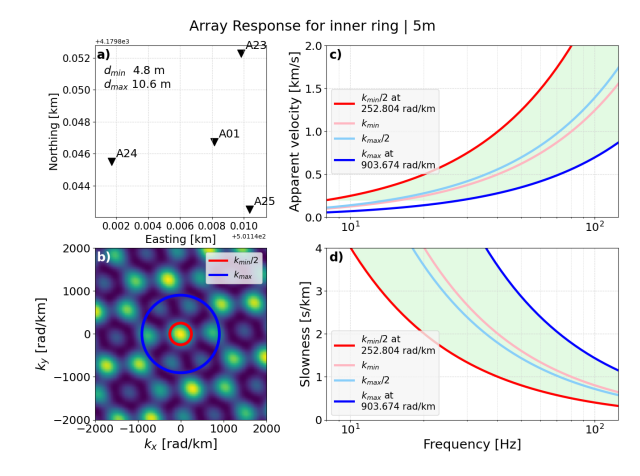


Figure 2.2: Array response for the largest ring of $100\ m$ radius. Panel a) shows the array configuration for the largest ring. Below, in panel b), the transfer function as a function of the wavenumber is found. The range of slownesses/velocities and frequencies that the configuration is sensitive to is highlighted by the bright green area while the dark red and dark blue curves represent the upper and lower limit of the response (panels c) and d)). Frequencies < 5Hz can be resolved.

50

51

52

53

54

55

Figure 2.3: Same set up as in figure 2.2 now focussing on the smallest ring. Frequencies $\sim 100 Hz$ can be resolved.

The locations of the arrays were significantly constrained by accessibility within the summit region. Two arrays were installed in close proximity to BNC, one of which was co-located with a broadband station of the linear profile, while other two were installed near the North-East Crater (NEC) providing full coverage of the central summit craters. A large section around the South-East Crater (SEC) was not accessible; thus, the remaining two arrays were deployed at slightly larger distance from the summit in the North and Northeast direction.

The most interesting results were obtained by the two arrays and linear array closest to BNC.

A more detailed view of the station configuration around BNC is shown in figure 2.4.

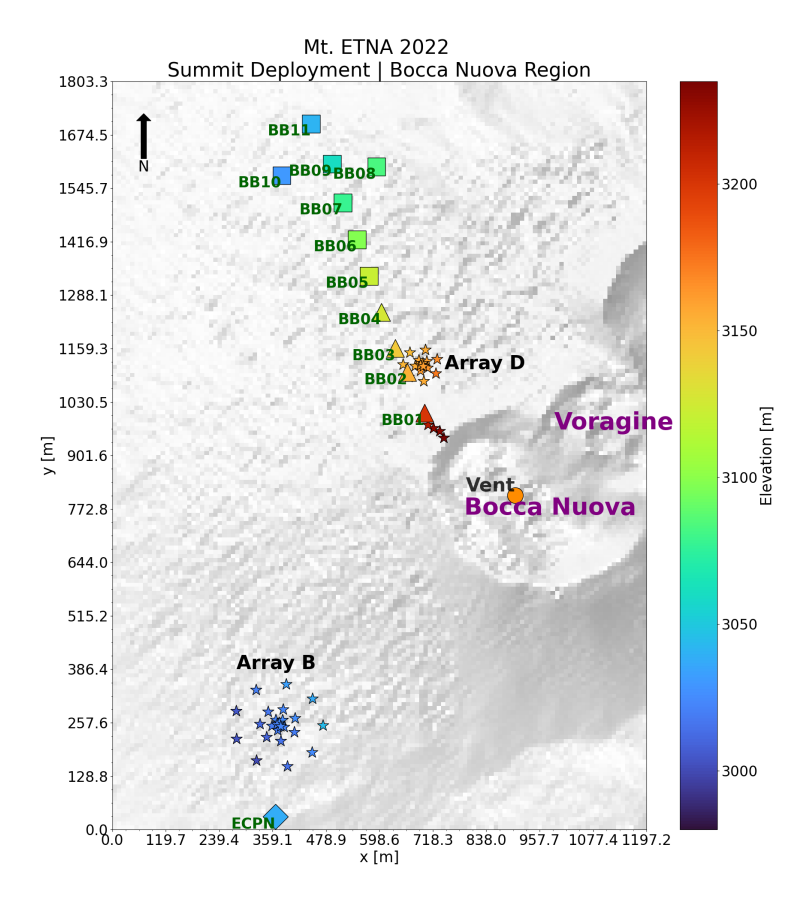


Figure 2.4: Zoomed-in view of the station set-up near BNC during the campaigns in summer 2022 focusing on the two Arrays B and D (25 and 16 short period instruments, respectively) as well as the linear array of short-period, broadband and infrasound stations leading up to the rim of BNC.

3. Episodic high-frequency tremor near the summit craters

59

61

The geometry of our arrays, and their proximity to the summit craters, is geared towards detection of tremor signals at frequencies of 10-20Hz. We detected several occurrences of 60 rarely observed tremor at approximately 12-15 Hz appearing in short-duration episodes, lasting minutes to about half an hour each (see figure 3.1).

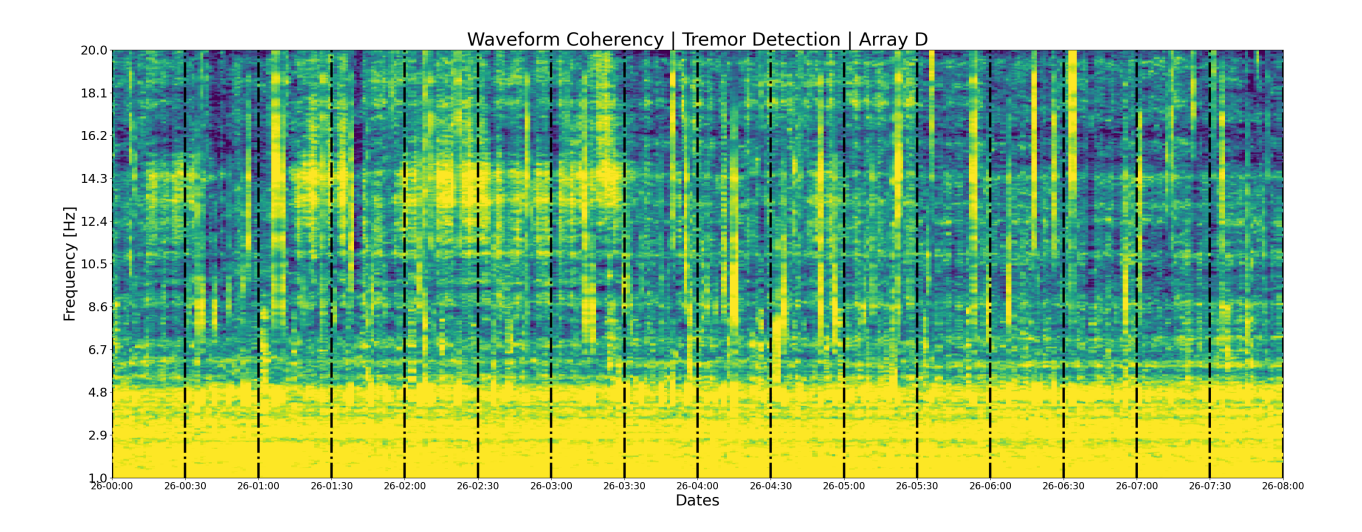


Figure 3.1: 8-hour record showing the waveform coherency obtained for all 16 short period stations in Array D closest to BNC revealing episodic high-frequency tremor (yellowish patches representing increased coherency) as well as the typical ever-present Etna-tremor below 5Hz. The dashed vertical lines mark 30-minute windows.

We use the COVSEISNET tremor detection tool developed by [10] and [11]. This approach divides the seismic traces across a network or array into sub-windows of which a certain number of adjacent windows are averaged after spectral whitening is applied to the traces. After transforming the signals into the frequency domain, their cross-spectra are calculated between all station combinations yielding the Covariance Matrix of dimensions $N \times N \times f \times t$ where N refers to the number of stations, f to frequency and t to time, respectively. The cross-spectra are calculated on individual subwindows while the Covariance matrix represents the average of all cross-spectra for a certain number of consecutive subwindows. Figure 3.1 shows the background low-frequency tremor typically reported at Mt. Etna ([8]) at frequencies below 5Hz. Very distinctive short-duration episodes of tremor are also visible primarily in the 12-15Hz band between 01:00 and 03:30 emerging from uncorrelated background noise. The episodic nature of the high-frequency signal, in contrast to the continuous appearance of the low-frequency tremor, suggests that their source mechanisms are likely different.

4. Time evolution of seismic and acoustic signals

Figure 4.1 shows the temporal evolution of seismic energy in the frequency band 12-15 Hz (Panel (a)). We plot the median amplitudes for non-overlapping 10-minute windows averaging all stations from Array D, the closest to the summit craters (see figures 2.4 and 2.1). The median amplitudes across the entire deployment are indicated as dashed lines. There is a long-term trend clearly visible with stronger seismicity registered early which then decreases below the respective means (dashed lines) before gradually increasing again in the second half of the deployment. This leads up to a second maximum in seismic energy recorded shortly before the instruments were retrieved. There are also significant short-term variations related to bursts or episodes of high-frequency tremor which are strongest near both the beginning and end of the deployment period.

Firstly, we were interested in how the high-frequency tremor band correlates with "typical" tremor at Mt. Etna. In the past, tremor at Mt. Etna has mainly been reported in the band 1-5Hz [8]. The temporal evolution of the signal in this band during our deployment is plotted

in Panel (b). A very similar long-term trend across the deployment period is clearly noticeable suggesting a potential link between the processes generating seismicity in both frequency bands. Closer inspection though reveals clear differences at shorter time scales. This can be observed 92 from the seismic ratio (12-15Hz vs. 1-5Hz, see Panel (e)) - this ratio shows a constant long-93 term behaviour, however, exhibits strong short-term variations (also note logarithmic y-axis 94 scaling). For example, one of the strongest high-frequency tremor episodes recorded between 95 01:00 and 04:00 in the morning of 26th August is not matched by such high energy levels in the 96 1-5Hz band. Similarly, another high-frequency tremor burst found at 20:00 on 30th August 97 is not accompanied by any increase in amplitudes between 1-5Hz. A mismatch between the 98 two frequency bands is also observed between 22:00 on the 29th and 06:00 on the 30th, when 99 quasi-periodic peaks similar in duration and amplitude are observed in the 1-5Hz range, but 100 not matched in the 12-15Hz band. These incidences indicate that tremor at 12-15Hz is unlikely 101 to be directly triggered by the same source mechanism driving the typical tremor < 5Hz but 102 may be treated as a separate signal, even though a similar long-term trend is found. 103 As discussed previously, volcanic tremor at Mt. Etna is frequently associated with degassing 104 activity, which would also present an acoustic signature. Even though Mt. Etna's overall activ-105 ity was very weak during the deployment both BNC as well as SEC were, in fact, continuously 106 degassing. The temporal evolution of infrasound amplitudes recorded at station BB05, the 107 closest to Array D (see figure 2.4), is plotted in the Panels (c) and (d). Signal median values 108 are shown for 10-minute windows (purple graphs) filtered between 3-5Hz and 12-15Hz bands, 109 respectively, with overall median added as a dashed line. Additionally, the pink graph displays 110 data filtered between 15-30 Hz serving as a proxy for potential acoustic noise linked to strong 111 winds and rainfall during the deployment. Infrasound stations were dismantled one day earlier 112 than the seismic stations, hence the gap in acoustic data towards the end of the deployment 113 period. 114

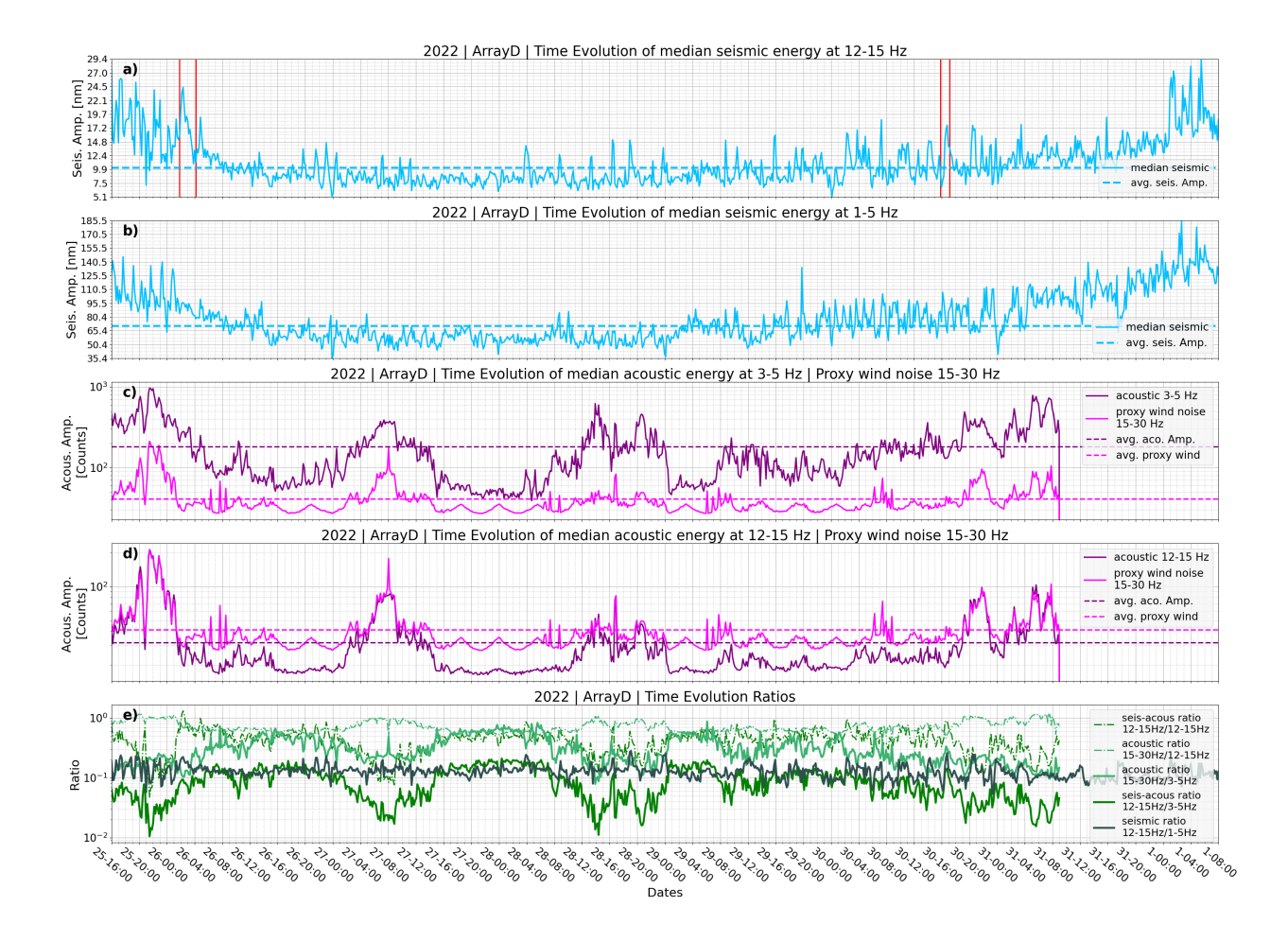


Figure 4.1: Evolution over time for seismic (Panel (a), $12-15\ Hz$ and Panel (b), $1-5\ Hz$) and acoustic energy (Panel (c), $3-5\ Hz$ and Panel (d), $12-15\ Hz$) recorded in various frequency bands of interest and their ratios (Panel (e)) during the entire short period instrument deployment for all stations of Array D. Two sections are marked by red vertical lines in panel a) which are closely investigated in figures 5.1, 5.3 and 5.4.

115

116

117

118

119

120

121

122

123

124

125

126

127

128

129

130

131

The 3-5 Hz band was deemed the most interesting owing to its occasional correlation with high-frequency tremor amplitudes, e.g. we find a high level of acoustic energy accompanying high-frequency tremor, which then decreases significantly as the high-frequency tremor does too (note logarithmic scale in acoustic panel). Acoustic energy increases gradually during the second half of the deployment similar to the seismic amplitudes. It should be noted though, that especially between 20:00 on 25th August and midnight acoustic energy levels are very high across broad ranges indicated by the red curve suggesting that atmospheric disturbances may have contributed to the very high amplitude level at 3-5 Hz at that time. On the other hand, we find two more periods (02:00 to 14:00 on 27th and 08:00 to midnight on 28th) of increased acoustic energy at 3-5 Hz. However, these two periods do not coincide with increased seismic amplitudes similar to those towards the beginning and end of the deployment. While the period between 05:00 and 10:00 on 27th August may also be affected by weather conditions as noise increases significantly between 15-30 Hz the other before-mentioned period on 28th shows very little sign of atmospheric noise pollution. Interestingly though, if degassing was intensifying at the time generating stronger acoustic signals at 3-5 Hz, this did not have a noticeable effect on the seismic output of the low- or high-frequency range. This is different to what is observed at the beginning and end of the deployment when the increased acoustic amplitudes coincide with increased seismic amplitudes. These variations hint at a complex relationship between seismic output and acoustic emissions.

5. Characterising episodic high-frequency tremor

During the six day-long deployment of short-period instruments we detected about 50 short-duration episodes of high-frequency tremor within the 12-15 Hz band ranging between several minutes to over half an hour (see figure 3.1). While [9] or [5] report on volcanic tremor observed > 10Hz on Mt. Etna and Fogo Volcano, Cape Verde Islands, tremor recorded at such high frequencies remains a rare observation. There are substantial differences between the tremor signals described in [9], which have a repetitive nature and stable durations, and the high-frequency tremor that we observe; our high-frequency tremor signals do not exhibit repetitive behaviour and have variable durations. [5] discuss harmonic tremor showing regularly spaced spectral bands which we also do not observe.

Below, we will investigate examples of high-frequency tremor in more detail looking into three tremor episodes within the highlighted parts in figure 4.1 that showcase the complexity and variability of these signals at Mt. Etna.

5.1. Case 1: High-frequency seismic tremor accompanied by acoustic signal across various frequency bands

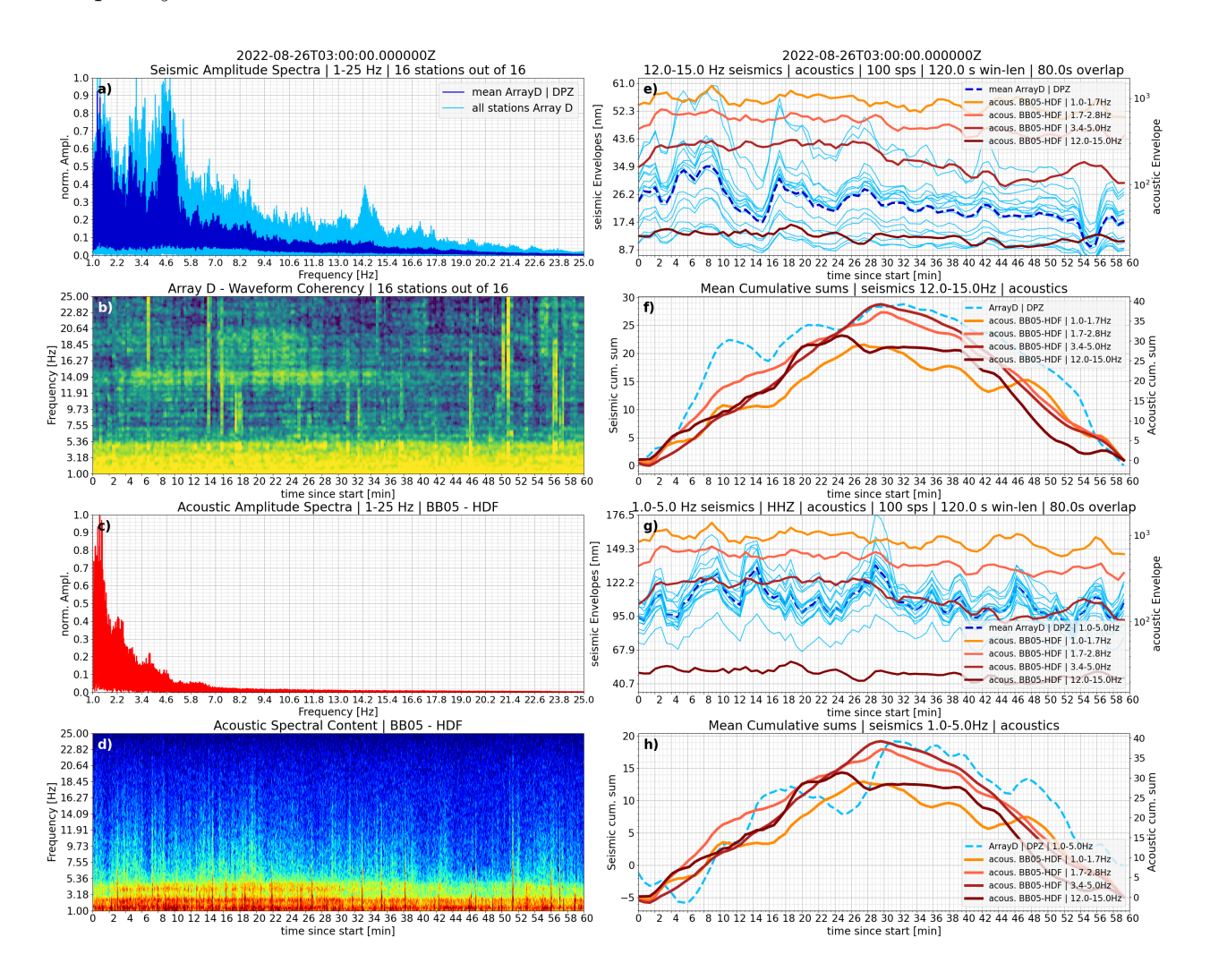


Figure 5.1: Detailed overview of a one-hour episode of high-frequency tremor, including spectral, amplitude, and trend analysis in both time and frequency domains. Panels (a) and (b) show the seismic spectra and waveform coherency-based tremor detection, respectively. Acoustic spectral content is displayed in panels (c) and (d). Panels (e)–(h) present the temporal evolution of amplitude envelopes and cumulative trends across various frequency bands. In panel (e), the thin solid bright blue lines represent individual stations from Array D (comprising 16 stations). All panels (e)–(h) use dual y-axes: the left y-axis corresponds to seismic data, and the right y-axis to acoustic data. This figure layout is consistent with the subsequent case studies shown in figures 5.3 and 5.4.

The first example, shown in Figure 5.1, presents an episode of high-frequency tremor recorded between 03:00 and 04:00 UTC on 26 August during the deployment period. Panel (b) shows waveform coherency computed across all stations in Array D using the COVSEISNET tremor detection tool ([10] and [11]), as previously introduced in Figure 3.1. The tremor band between 12-15Hz is clearly variable in intensity and is strongest during the interval from approximately 3 to 28 minutes into the one-hour period. Adjacent frequency bands also show a slight increase in coherent signal content compared to the uncorrelated background noise. This 12-15Hz tremor band dominates the amplitude spectrum, with a prominent spectral peak around 14Hz visible in Panel (a). Additionally, both Panels (a) and (b) capture

the presence of the characteristic "Etna tremor" between 1-5Hz, which reaches substantially higher amplitudes (refer to displacement axes in Panels (e) and (g) for high- and low-frequency ranges, respectively).

High-frequency tremor is also apparent in Panel (e), where the seismic envelopes decrease significantly in tandem with the drop in coherent energy detected in Panel (b). The envelopes are calculated using 120-second windows with a two-thirds overlap, applying the median to suppress impulsive events from degassing craters BNC and SEC.

Panel (a) further highlights the strong attenuation of high-frequency content over short distances, particularly in heterogeneous environments such as volcanic edifices. The thin blue lines in the spectrum represent the 16 individual stations of Array D and illustrate a wide spread in amplitudes—ranging from 15 to 60nm —at around 8 minutes into the time window, despite an array aperture of only 80m.

Panels (c) and (d) show the acoustic spectral content at station BB05 and its temporal evolution, respectively. Three prominent spectral peaks are visible at 1.3, 2.2, and 3.8Hz. Notably, the 3.8Hz peak in Panel (d) shows a striking similarity in its temporal evolution to the high-frequency seismic tremor in Panel (b): it is weak at first, intensifies after minute 3, and then fades after minute 28.

To highlight this similarity, the cumulative trends for the relevant frequency bands are shown in Panel (f), after zero-meaning and normalisation by standard deviation. The seismic content filtered at 12-15Hz (dashed bright blue line) and the acoustic band at 3.4-5Hz (solid orange line) show nearly identical trends, supporting the visual impression from Panels (b) and (d) and suggesting a correlation between the two signals. It should be noted here though that, even other acoustic bands —including 12-15Hz, where the seismic tremor is found — exhibit similar cumulative trends in this example.

The most striking observation is that the frequency ranges of these temporally correlated seismic and acoustic signals differ: 12-15Hz (seismic) versus 3-5Hz (acoustic). This suggests that low-frequency acoustic emissions may be linked to the high-frequency seismic tremor through a common driving process, as inferred from the shared amplitude trends over time. Additionally, a potential connection to low-frequency seismic tremor cannot be excluded, given the similarities in cumulative trends shown in Panel (h).

A key question arises: How can this close temporal match between high-frequency seismic 189 tremor and low-frequency acoustic signals be explained? Given the distinct frequency ranges, 190 it is likely that the two signals are generated by separate processes that are nonetheless linked 191 due to their match in time. A non-linear transition of energy from air to solid medium causing 192 a frequency shift can be ruled out, as helicopter-produced signals are consistently recovered on 193 both acoustic and seismic channels at the same expected frequencies (see Figure 5.2). Similar 194 to the findings of [12], we observe gliding acoustic tremor patches and associated overtones 195 from helicopters flying over the volcano, particularly in the morning and afternoon. 196

Taken together, these observations strongly support the interpretation that high-frequency seismic tremor and low-frequency acoustic signals are generated by separate, but temporally linked, physical processes.

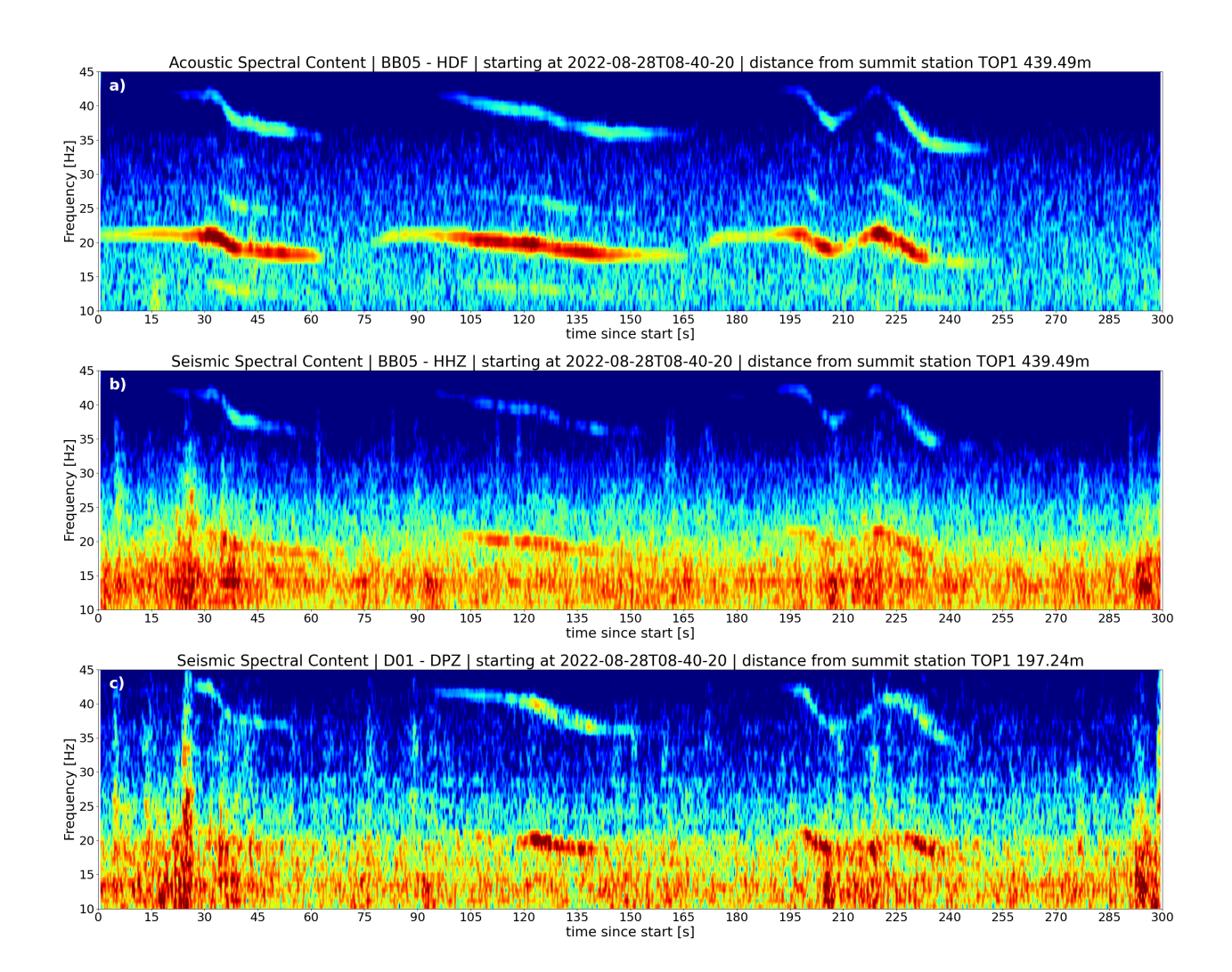


Figure 5.2: Gliding tremor observed from a helicopter passing over the summit of Mt. Etna. Panel (a) shows the acoustic spectrum, clearly revealing both the fundamental frequency and its overtones. The data is filtered between 10-45Hz, highlighting the helicopter-induced gliding tremor at consistent frequencies. The signal is even more pronounced at a short-period seismic station, as shown in Panel (c). Distances from the summit reference station (BNC) are indicated in the titles of the respective panels.

5.2. Case 2: High-frequency tremor episode matched well by 3-5Hz acoustic band

This case investigates the strongest high-frequency tremor episode recorded between 02:00 and 03:00 UTC on 26 August (Figure 5.3). Coherent tremor energy, primarily within the 12-15Hz band, is detected throughout the entire one-hour period, with maximum intensity observed between minutes 4 and 36, as shown in Panel (b) and confirmed by the amplitude envelopes in Panel (e). The spectral peak near 14Hz, shown in Panel (a), is the most prominent across all cases examined.

Three distinct spectral peaks in the acoustic signal—at approximately 1.3Hz, 2.2Hz, and 3.8Hz—are clearly visible again in Panel (c), similar to Case 1. Additionally, the 3-5Hz acoustic band is strongly expressed in the acoustic spectrogram (Panel (d)) and exhibits a temporal evolution that closely matches the high-frequency seismic tremor observed in Panel (b).

Given that this episode occurred only one hour prior to the one analysed in Case 1, it is not surprising that the key observations are largely consistent between the two cases. The

cumulative trends for the 12-15Hz seismic band and the 3-5Hz acoustic band (Panel (f)) align closely during the interval of strongest tremor activity. However, in contrast to Case 1, the trends diverge more significantly outside this period. Notably, the other acoustic bands show far less agreement with the seismic trend, and the 12-15Hz acoustic band in particular behaves quite differently from its seismic counterpart. This reinforces the interpretation that the strongest correlation exists specifically between the 12-15Hz seismic band and the 3-5Hz acoustic band.

Unlike in Case 1, the low-frequency seismic content (<5Hz) deviates more clearly from the high-frequency seismic tremor in this case, suggesting that the typical Etna tremor and these high-frequency signals may be driven by separate processes.

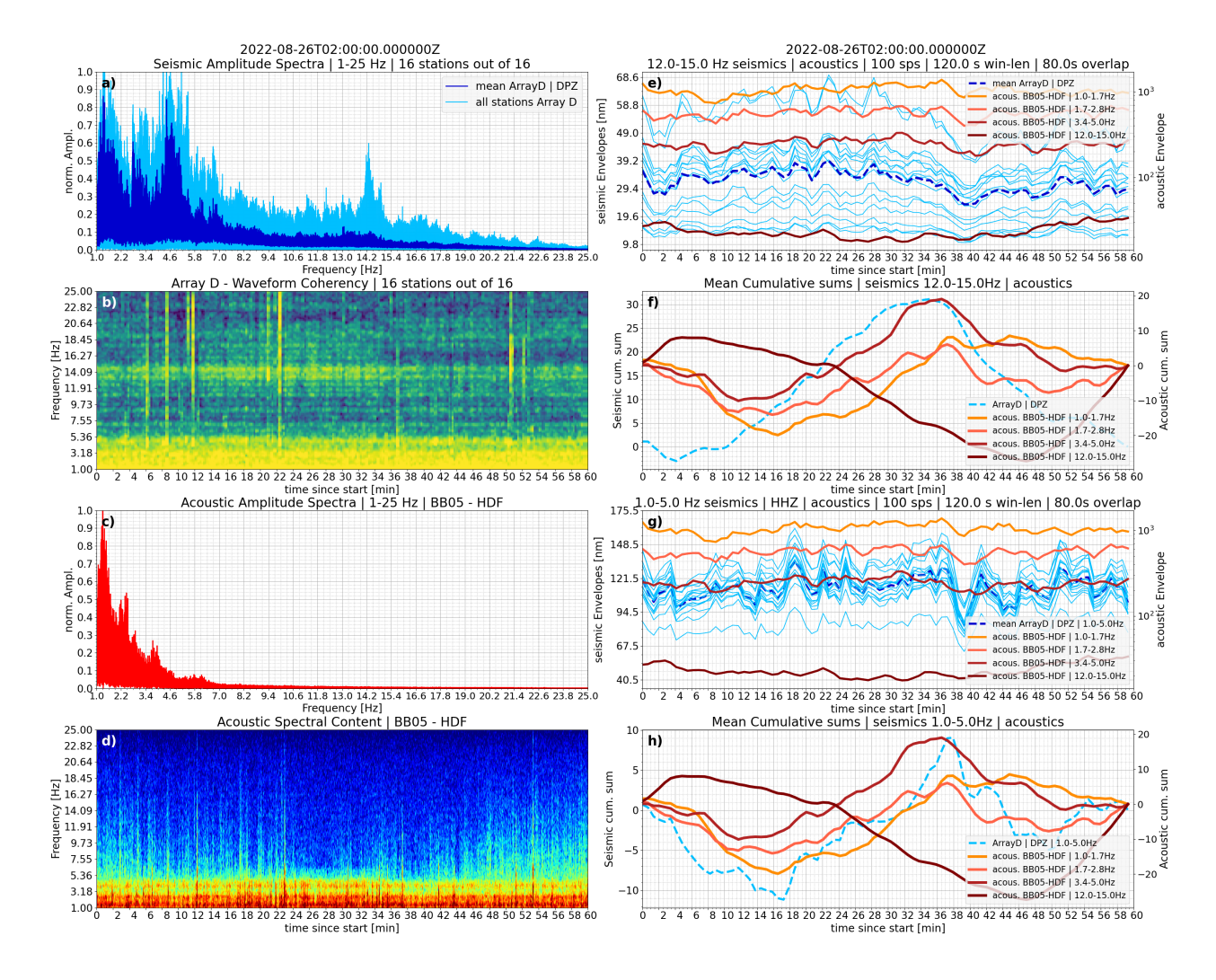


Figure 5.3: Detailed overview of a second 1-hour long episode of high-frequency tremor.

5.3. Case 3: High-frequency seismic tremor not matched by acoustic signal

This final case study examines the one-hour interval between 16:00 and 17:00 UTC on 30 August (Figure 5.4). It captures another strong high-frequency tremor episode, beginning around minute 21 and lasting for over half an hour. The episode is clearly visible in the waveform coherency plot Panel (b) and the seismic amplitude envelopes Panel (e). As in previous cases, adjacent frequency bands also exhibit increased coherent energy, and a prominent spectral peak is again observed near 14Hz Panel (a).

However, this example displays a notable deviation from Cases 1 and 2. Specifically, the 3-5Hz230 acoustic band—previously well-expressed—is largely absent here. No distinct peak is observed 231 in the acoustic spectrum Panel (c), and the spectrogram Panel (d) shows no significant energy 232 in this band during the high-frequency seismic tremor. Importantly, the seismic amplitude of 233 this episode is comparable to that of Case 1, suggesting that the absence of the 3-5Hz acoustic 234 signature cannot be attributed to a weaker tremor (see Panel (e) and compare with Figure 5.1). 235 As a result, the cumulative trend of the 12-15Hz seismic band diverges markedly from that 236 of the 3-5Hz acoustic band, and no other acoustic band shows a matching trend either Panel 237 (f). Additionally, the low-frequency seismic content (< 5Hz), typically associated with Etna 238 tremor, exhibits an opposing trend, further indicating a decoupling of low- and high-frequency 239 components in this case. 240

The absence of the 3-5Hz acoustic signal—previously interpreted as a likely indicator of degassing activity ([13]) — suggests that the process generating this acoustic emission may not be essential for the occurrence of high-frequency tremor. This raises the possibility that in this case, the tremor may be triggered independently of degassing, questioning whether fluid migration processes are directly involved.

As noted in Case 1, the acoustic signature of a helicopter overflight is also present in this episode Panel (d), visible between 18 and 22Hz from minutes 36 to 41. Additionally, a faint indication of a secondary gliding tremor patch appears near 14Hz at approximately minute 36, possibly related to the same overflight event.

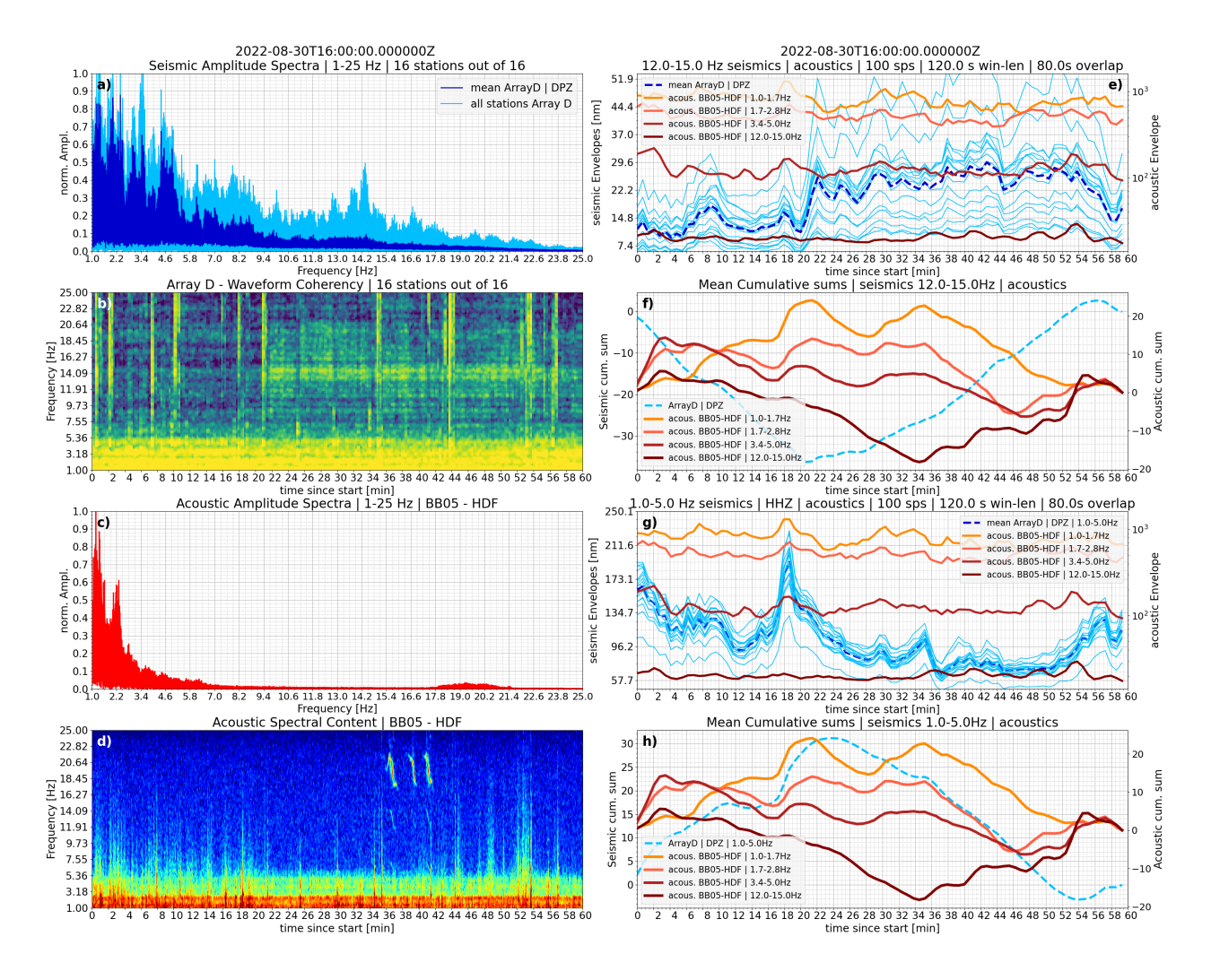


Figure 5.4: Detailed overview of a third episode of high-frequency tremor (1 hour of data). Here, the accompanying acoustic signal at 3-5Hz observed before is largely missing.

6. Variability of seismic-acoustic correlations

As shown in the previous case studies, a potential seismic–acoustic correlation between the 12-15Hz seismic tremor and the 3-5Hz acoustic signal can be observed, but it is not consistent across all examples. To better illustrate the complexity and variability encountered when jointly analysing the seismic and acoustic data, we plot the median amplitudes of 10-minute non-overlapping time windows for the frequency bands of interest against one another (Figure 6.1).

Panel (a) displays the relationship between the 12-15Hz seismic tremor and the 3-5Hz acoustic signal, with acoustic amplitudes plotted as a function of seismic amplitudes. Overall, the correlation is weak, revealing considerable variability in acoustic energy for any given level of seismic activity, and vice versa. Nonetheless, a broad trend toward higher amplitudes in one signal when the other increases can be observed. However, this relationship is loose and not necessarily valid for individual cases—such as Case 3—highlighted here by the wide spread in the data. Most time windows fall within a relatively narrow range of seismic amplitudes (7-15nm), while the corresponding acoustic amplitudes range from 20 to over 400counts, a variation by more than a factor of 20.

As previously mentioned, atmospheric conditions such as wind or rainfall influence the acous-266 tic spectral content. To account for this, Panel (d) compares the 3-5Hz acoustic band with a 267 broader high-frequency acoustic band (15-30Hz), which is more sensitive to wind-induced noise. 268 The distribution shows that time windows with 3-5Hz acoustic amplitudes below $\sim 300 counts$ 269 are generally unaffected by atmospheric disturbances, as these coincide with low amplitudes in 270 the 15–30Hz band. In contrast, higher-amplitude outliers in the 3–5Hz band are often accom-271 panied by elevated energy in the 15-30Hz range, suggesting an atmospheric origin. Assuming 272 that the 3-5Hz acoustic amplitudes in the 25-300count range are primarily volcanic in origin, 273 the data indicate that high-frequency seismic tremor may be triggered under a range of con-274 ditions. As illustrated in Case 3 (Figure 5.4), strong high-frequency tremor may occur with 275 minimal accompanying acoustic energy, potentially implying weak or absent degassing during 276 such events — consistent with previous findings linking continuous degassing to low-frequency 277 acoustic tremor [13]. 278

Panel (b) shows no evidence of a systematic correlation between the 12-15Hz seismic and 12-15Hz acoustic bands, further supporting the idea that these frequency ranges are not directly coupled in the acoustic domain.

In Panel (c), a weak positive correlation is observed between the low-frequency (< 5Hz) and high-frequency (12-15Hz) seismic bands. However, the wide variation in amplitude ratios across the dataset suggests the absence of a simple linear relationship when analysing short time windows. Nevertheless, a broader long-term correlation may exist, as suggested by the trends observed in Figure 4.1.

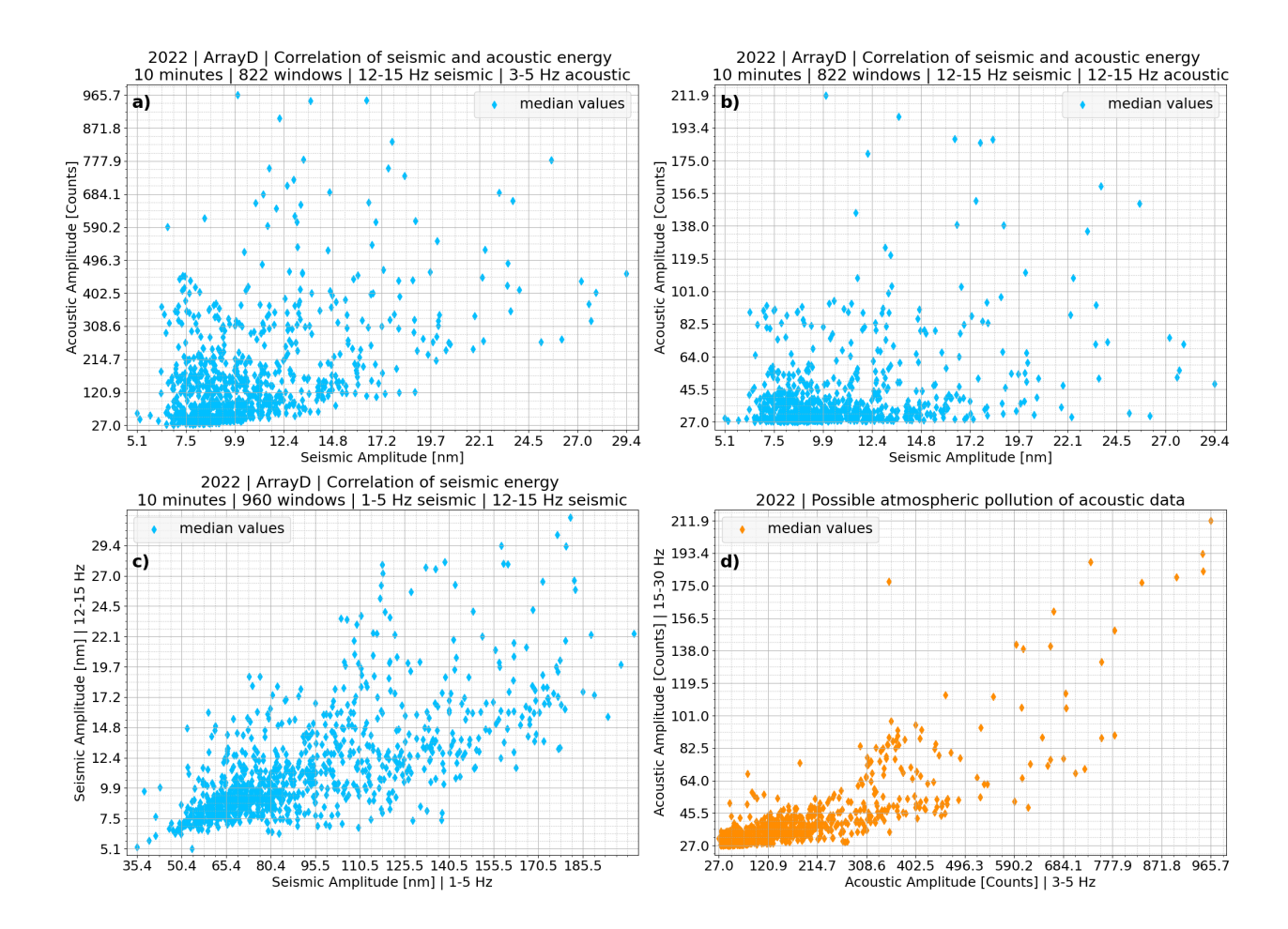


Figure 6.1: Median amplitudes calculated over 10-minute non-overlapping windows for selected frequency bands of interest. Panel (a) shows a scatter plot of the 3-5Hz acoustic band versus the 12-15Hz seismic band, using all available data from the large deployment between 25 August and 1 September. For comparison, Panel (b) plots the 12-15Hz acoustic band as a function of the high-frequency (12-15Hz) seismic tremor. Panel (c) compares the typical low-frequency Etna tremor (i5Hz) with the high-frequency tremor. Panel (d) evaluates the influence of atmospheric conditions on the acoustic data, highlighting potential weather-related variability.

7. Volcanic tremor's driving mechanisms

The above exemplifications form a picture of quite convoluted high-frequency tremor signals, which show a complex seismic-acoustic ratio and temporal evolution. The recovery of volcanic tremor at such high frequencies is a rare finding in itself with very few exceptions like [9] or [5] reporting on high-frequency tremor signals. Our findings here suggest that the high-frequency tremor may be generated under different circumstances as we see tremor exhibiting a high seismic-acoustic correlation but also recover specific tremor episodes which are lacking the correlation with acoustic data expected for tremor directly related to degassing (see figure 5.4). Moreover, the observed high-frequency tremor is seemingly identical in spectral characteristics and energy output regardless of the changing acoustic record. Interestingly, those examples of correlating seismic and acoustic data show different frequencies indicating two potential processes driving these signals which are likely linked due to their match in time.

7.1. Established models for volcanic tremor

300

301

302

303 304

305

306

307

308

309

310

311

312

314

315

316

317

318

319

320

321

322

323

324

325

327

328

329

330

331

332

333

334

335

336

337

338

340

341

342

Traditionally, the generation of volcanic tremor is attributed to processes involving mass transport (magma flow in volcanic conduits) as described in [14] or [15]. This link makes tremor a promising candidate for identifying and characterising unrest and forecasting eruptions at

A widely accepted source mechanism for volcanic tremor is sustained degassing activity (e.g., [16], [1]). Clear links have been demonstrated between persistent degassing and variable tremor amplitude at Mt. Etna in previous studies (e.g., [17, 18]). Seismic tremor at Mt. Etna is widely observed to frequently precede and accompany eruptive activity [19], confirming its potential use in eruption forecasting. [20], found that the correlation between the tremor amplitude and the SO_2 flux rates reaches its maximum during eruptive periods. The style of eruption has been shown to influence the characteristics of tremor signals ([21]). [13] identified persistent acoustic tremor associated with continuous volcanic degassing, attributing variations in tremor energy to resonance within gas-filled cavities and to fluctuations in degassing intensity. Despite numerous 313 studies linking tremor to magma or gas movement, these models fail to explain the observed range of tremor signals and their relation to other monitoring parameters. [22], for example, showed an inverse correlation between CO_2 flux rates and tremor recorded at Stromboli; [23], on the other hand, observed a time-lagged correlation between those parameters at Mt. Etna with tremor lagging behind degassing by about 50 days. [24] report the opposite at Soufriere Hills Volcano, Montserrat (WI), where gas flux lags behind tremor.

7.2. Non-fluid related driving mechanisms

One aspect is common to many of the models - they require the presence of fluids (magma, gases) involved in the processes that generate tremor. Several recent studies have challenged this hypothesis.

[25] demonstrated how seismicity of tremor-like character could be generated without invoking the presence of fluids at the source. The authors conduct numerical simulations for very low-cohesian and weak materials common on a volcanic edifices (e.g., [26] who studied deposits from Stromboli's upper edifice). The numerical simulations carried out are based on a model developed by [27] and they find that breaching a certain stress threshold leads to the continuous generation of low-amplitude, very small stress-drop seismic events so closely spaced in time that they appear as tremor and are related to a diffusive failure pattern. This observation is in agreement with the numerical results of [27] who studied the seismic output associated with changing angles of internal friction. On key finding is, that the seismic b-value of material of low angles of internal friction exhibits non-power-law scaling lacking larger events.

Very similar results are seen for a Long-Period (LP) seismicity catalogue from Mt. Etna acquired by [25] suggesting that the weak material making up the upper edifice is found near the brittle-ductile boundary. This merely supports low-amplitude seismicity merging into tremor due to diffusively damaged material across the edifice rather than localised ruptures as the weak material cannot sustain the required stress for larger events. [25] therefore propose that the swarms of LP events on Mt. Etna can be caused by quasi-brittle behaviour, as very small stress-drop events are triggered by deformation, that the edifice undergoes. Crucially, they point out that even if changes in stress levels occurring are contributed to by gas influx or magma migration, the failure process itself can be dry mechanical.

This concept is supported by laboratory experiments carried out by [28] who encounter tremor-343 like acoustic emissions from a sample of Napolitan Tuff under slow compression after having 344 been fully dried. Despite the complete absence of fluids, tremor-like signals are recovered and 345

the associated damage pattern is diffusive in character rather than localised.

7.3. Driving mechanisms of high frequency tremor in recorded signals?

The varying seismo-acoustic ratios observed in the different high-frequency tremor episodes clearly suggest that the tremor is triggered under various circumstances and thus a model linking the tremor directly to degassing is not sufficient to explain all incidences of tremor detected. Based on the numerical work by [27] as well as findings by [28] from laboratory tests on typical volcanic material we suggest a non-fluid related source mechanism needs to be considered here. As proposed by [25] the weak material with low angles of internal friction that the edifice is made up of may generate low-amplitude, tremor-train like signals due to quasi-brittle failure. We suggest a similar source mechanism may be causing these tremor episodes here. The tremor found in a high frequency band is suggestive of mesoscale failure generating a cascade of low amplitude low stress drop events that merge into tremor.

A key aspect to consider here are the different frequency bands for the high-frequency seismic tremor at 12-15Hz and the correlating acoustic signal which primarily dominates at 3-5Hz. As we have shown we do not expect any non-linear coupling of acoustic signals into solid medium towards higher frequencies as the acoustic helicopter signals are retrieved without any frequency shift in the seismic data similar to observations made by [12]. Therefore, we conclude that the observed different frequencies are almost certainly the result of two different processes which, however, are tied together through their temporal match observed for instance in figures 5.1 and 5.3). We propose that continuous passive degassing causes the 3-5Hz acoustic signal (similar to [13] linking oscillation of gases in cracks to acoustic tremor) while the escaping gases produce very small stress changes sufficient to trigger quasi-brittle failure of the very weak host rock which is picked up at 12-15Hz in the seismic data. However, considering the before mentioned examples of tremor lacking the acoustic correlation quasi-brittle failure may even be triggered without degassing present as discussed by [25].

To shed more light onto tremor possibly being purely deformation driven without a direct link to fluids further investigations are required, e.g. focusing on the source locations of the tremor episodes as tremor of this kind would be expected to be of a diffusive rather than localised nature and source areas would also not necessarily be confined to the degassing crater region but potentially be more spread out across the edifice.

8. Conclusion

We present a remarkably rich seismo-acoustic data set from the summit region of Mt. Etna containing rarely observed high-frequency short-duration episodes of tremor dominating in the 12-15Hz band. These tremor signals are found to show significantly varying seismic-acoustic amplitude ratios suggesting that different circumstances may lead to the triggering of high-frequency tremor. Therefore, degassing activity may not be sufficient to explain all of its occurring incidences. We propose that quasi-brittle, mesoscale failure of very weak material in the summit region may need to be considered as the direct source mechanism of the episodic tremor as suggested by several previous studies. Some of the high-frequency tremor seems to be indirectly driven by continuous degassing activity producing a time-matching acoustic signal at a different frequency. On the other hand, we find examples lacking the accompanying acoustic signal, potentially indicating degassing (and therefore involved fluids) is not required as a triggering process as it appears to be absent at the time. It can not be ruled out though,

that gases are still accumulating causing small stress level changes ultimately leading to material damage producing high-frequency seismic tremor while the gases are unable to escape. Crucially, we assume that even if degassing indirectly triggers the seismic tremor, the actual source mechanism producing the tremor signal would be dry mechanically to account for the different frequency at which the seismic tremor is observed as opposed to the acoustic signal. We are currently conducting further investigations into tremor source locations, to improve our understanding of the phenomenon.

9. Acknowledgements

We want to thank the IMPROVE European Horizon's 2020 research and innovation programme as well as the SINFONIA project under which the fieldwork acquiring this data was carried out. Furthermore, we would like to thank numerous people for helping during the field campaigns to Mount Etna in summer 2022 who are Vittorio Minio, Elisabeth Glueck, Regina Maass and Eleanor Dunn.

403 References

- [1] K. I. Konstantinou, V. Schlindwein, Nature, wavefield properties and source mechanism of volcanic tremor: a review, Journal Volcanolology and Geothermal Research, Volume 119, Issues 1-4, 161-187 (2002).
- [2] G. G. Salerno, M. Burton, G. D. Grazia, T. Caltabiano, C. Oppenheimer, Coupling between magmatic degassing and volcanic tremor in basaltic volcanisms, frontiers in Earth Science, Volume 6, Article 157 (2018).
- [3] L. Chardot, A. D. Jolly, B. M. Kennedy, N. Fournier, S. Sherburn, Using volcanic tremor for eruption forecasting at white island volcano (whakaari), new zealand, Journal Volcanolology and Geothermal Research, Volume 302, 11-23 (2015).
- [4] S. R. McNutt, Volcanic tremor, Encyclopedia of Earth System Science, Volume 4 (1992).
- [5] S. I. Heleno, B. V. Faria, Z. Bandomo, J. F. Fonseca, Observations of high-frequency harmonic tremor in fogo, cape verde islands, Journal Volcanolology and Geothermal Research, Volume 158, Issues 3–4, 361-379 (2006).
- [6] T. Permana, T. Nishimura, H. Nakahara, E. Fujita, H. Ueda, Reliability evaluation of volcanic tremor source location determination using cross-correlation functions, Geophysical Journal International, Volume 220, 1300–1315 (2019).
- [7] J. M. Ibanez, I. Castro-Melgar, O. Cocina, L. Zuccarello, S. Branca, E. D. Pezzo, J. Prudencio, First 2-d intrinsic and scattering attenuation images of mt etna volcano and surrounding region from active seismic data, Geophysical Journal International, Volume 220, 267–277 (2019).
- [8] B. D. Lieto, G. Saccorotti, L. Zuccarello, M. L. Rocca, R. Scarpa, Continuous tracking of volcanic tremor at mount etna, italy, Geophysical Journal International, Volume 169, Issue 2, 699-705 (2007).

- 427 [9] A. Cannata, G. D. Grazia, P. Montalto, F. Ferrari, G. Nunnari, D. Patanè, E. Privit-428 era, New insights into banded tremor from the 2008–2009 mount etna eruption, Journal 429 Volcanolology and Geothermal Research, https://doi.org/10.1029/2009JB007120 (2010).
- [10] L. Seydoux, N. Shapiro, J. de Rosny, F. Brenguier, M. Landes, Detecting seismic activity with a covariance matrix analysis of data recorded on seismic arrays, Geophysical Journal International, Volume 204, 1430–1442 (2016).
- [11] J. Soubestre, N. M. Shapiro, L. Seydoux, J. de Rosny, D. V. Droznin, S. Y. Droznina,
 S. L. Senyukov, E. I. Gordeev, Network-based detection and classification of seismovol canic tremors: Example from the klyuchevskoy volcanic group in kamchatka, Journal of
 Geophysical Research: Solid Earth, https://doi.org/10.1002/2017JB014726 (2018).
- [12] E. P. S. Eibl, I. Lokmer, C. J. Bean, E. Akerlie, K. S. Vogfjörd, Helicopter vs. volcanic tremor: Characteristic features of seismic harmonic tremor on volcanoes, Journal of Volcanology and Geothermal Research, 304, 108–117 (2015).
- [13] D. Fee, M. Garcés, M. Patrick, B. Chouet, P. Dawson, D. Swanson, Infrasonic harmonic
 tremor and degassing bursts from halema'uma'u crater, kilauea volcano, hawaii, Journal
 Geophysical Research, Vol. 115, B11316 (2010).
- [14] G. S. Steinberg, A. S. Steinberg, On possible causes of volcanic tremor, Journal Geophysical Research, https://doi.org/10.1029/JB080i011p01600 (1975).
- [15] J. Neuberg, T. Pointer, Effects of volcano-topography on seismic broadband waveforms.
 Geophysical Journal International, Volume 143, Issue 1, 239–248 (2000).
- 447 [16] G. Williams-Jones, J. Stix, M. Heiligmann, J. Barquero, E. Fernandez, E. D. Gonzalez,
 A model of degassing and seismicity at arenal volcano, costa rica., Journal Volcanolology
 and Geothermal Research, Volume 108, Issues 1–4, 121-139 (2001).
- [17] S. Gresta, A. Montalto, G. Patanè, Volcanic tremor at mount etna (january 1984–march
 1985): its relationship to the eruptive activity and modelling of the summit feeding system,
 Bull. Volcanol. Volume 53, 309–320 (1991).
- tween very long period seismic events, volcanic tremor, and degassing rates at mount etna volcano, Journal Geophysical Research, Solid Earth Volume 118, 4910–4921 (2013).
- 456 [19] A. Cannata, A. Catania, S. Alparone, S. Gresta, Volcanic tremor at mt. etna: inferences 457 on magma dynamics during effusive and explosive activity, Journal Volcanolology and 458 Geothermal Research, Volume 178, Issue 1, 19–31 (2008).
- ⁴⁵⁹ [20] S. Leonardi, S. Gresta, F. Mulargia, Cross-correlation between tremor and so2 flux data from mount etna volcano, 1987-1992, Phys. Chem. Earth, Volume 25, 737–740 (2000).
- 461 [21] A. Cannata, G. D. Grazia, M. Giuffrida, S. Gresta, M. Palano, M. S. et al., Space-time evolution of magma storage and transfer at mt. etna volcano (italy): the 2015/2016 reawak-ening of voragine crater, Geochem. Geophys. Geosys. Volume 19, 471–495 (2018).
- ⁴⁶⁴ [22] A. Aiuppa, M. Burton, T. Caltabiano, M. Ripepe, Anti-correlation between gas flux and volcanic tremor on stromboli volcano, EGU General Assembly 2009, p.13671 (2009).

- 466 [23] A. Cannata, G. Giudice, S. Guerrieri, P. Montalto, S. Alparone, G. D. G. et al., Relationship between soil co2 flux and volcanic tremor at mt. etna: implications for magma dynamics, Environ. Earth Sci. Volume 61, 477–489 (2009).
- 469 [24] S. R. Young, B. Voight, H. J. Duffell, Magma extrusion dynamics revealed by high-fre-470 quency gas monitoring at soufrière hills volcano, monserrat, Geol. Soc. Spec. Publ. Volume 471 213, 219–230 (2003).
- 472 [25] C. J. Bean, L. D. Barros, I. Lokmer, J.-P. Métaxian, G. O. Brien, S. Murphy, Long-period 473 seismicity in the shallow volcanic edifice formed from slow-rupture earthquakes, Nature 474 Geoscience, DOI: 10.1038/NGEO2027 (2013).
- ⁴⁷⁵ [26] T. Apuani, C. Corazzato, A. Cancelli, A. Tibaldi, Physical and mechanical properties of rock masses at stromboli: A dataset for volcano instability evaluation, Bull. Eng. Geol. Environ. Volume 64, 419–431 (2005).
- 478 [27] D. Amitrano, Brittle-ductile transition and associated seismicity: Experimental and numerical studies and relationships with the b value, J. Geophys. Res. Volume 108, 2044–2059 (2003).
- ⁴⁸¹ [28] P. Rowley, P. M. Benson, C. J. Bean, Deformation-controlled long-period seismicity in low-cohesion volcanic sediments, Nature Geoscience, https://doi.org/10.1038/s41561-021-00844-8 (2021).